

Non-Invasive Bladder Volume Monitoring via Pelvic Bioimpedance

3D FEM Simulation with SVD-Optimal Electrode Drive Patterns

Abstract

We present a 3D finite-element simulation of pelvic bioimpedance for non-invasive bladder volume monitoring. The model includes 15 tissue types with frequency-dependent conductivities, the Complete Electrode Model for realistic electrode contact, and anisotropic volume-dependent bladder geometry based on ultrasound literature. We compare two practical configurations using the same 8-electrode suprapubic belt: (1) conventional 4-electrode tetrapolar measurement at $0.22\text{ m}\Omega/\text{mL}$, and (2) SVD-optimal 8-electrode drive patterns at $0.94\text{ m}\Omega/\text{mL}$ —a $4.3\times$ improvement requiring only a firmware change. A complete signal processing algorithm (band-stop respiratory filter, low-pass cardiac filter, polynomial detrending, void-event calibration) extracts the bladder filling trend from artifacts. BMI analysis confirms that a single set of SVD drive weights achieves $> 98\%$ efficiency across all body types. The 8-electrode SVD configuration meets the clinical target of $0.1\text{ mL}/(\text{kg h})$ ($\sim 7\text{ mL}$ at 70 kg) with $\sim 6\text{ mL}$ resolution.

Contents

1	Introduction	3
2	Anatomical Model	3
2.1	Torso Geometry	3
2.2	Tissue Properties	3
2.3	Bladder Geometry	3
2.4	Complete Electrode Model	3
3	Electrode Placement	5
3.1	Configuration Sweep	5
3.2	The Belt	5
4	Optimal 4-Electrode Configuration	5
4.1	The Sensitivity Ceiling	6
4.2	Optimal 4-Electrode Pair	6
5	Optimal 8-Electrode Configuration: SVD Drive Patterns	6
5.1	The Idea	6
5.2	Construction	7
5.3	Why SVD, Not Simple Sensitivity Weighting	7
6	Signal Processing Algorithm	9
6.1	Stage 1: Band-Stop Filter (0.15 Hz to 0.4 Hz)	9
6.2	Stage 2: Low-Pass Filter ($< 0.08\text{ Hz}$)	9
6.3	Stage 3: Polynomial Baseline Detrending	9
6.4	Stage 4: Calibration and Volume Estimation	9

6.5	Complete Algorithm	10
7	Multi-Frequency Analysis	11
7.1	Beta Dispersion and Spectral Unmixing	11
7.2	Why It Fails	11
7.3	Dual-Frequency Subtraction	11
8	BMI Sensitivity Analysis	12
9	Noise Budget and Accuracy	14
9.1	Noise Sources	14
9.2	Volume Resolution	14
10	Anterior-Only Placement	15
11	Clinical Implementation	16
11.1	Hardware	16
11.2	Expected Performance	17
11.3	Upgrading to 16 Electrodes	17
12	Limitations	17
13	Conclusion	17

1 Introduction

Urine output is a core vital sign for assessing kidney function in hospitalized patients. The clinical target of $0.1 \text{ mL}/(\text{kg h})$ corresponds to 7 mL at 70 kg body weight. Current monitoring requires an indwelling urinary catheter, which carries a 3–5% daily risk of catheter-associated urinary tract infection (CAUTI).

Bioimpedance offers a non-invasive alternative: surface electrodes inject a small alternating current (1 mA at 50 kHz) and measure the resulting voltage. As the bladder fills with conductive urine (1.75 S/m), the measured impedance changes. The challenge is that the bladder sits deep in the pelvis—approximately 6.7 cm behind skin, fat, muscle, and bone—and the impedance change per millilitre of urine ($0.2 \text{ m}\Omega/\text{mL}$ to $1.0 \text{ m}\Omega/\text{mL}$) is buried under respiratory artifacts that are $100\times$ larger.

This report presents a simulation study comparing two electrode configurations using the same 8-electrode suprapubic belt:

- **4-electrode tetrapolar:** use 4 of the 8 electrodes in a standard 4-wire measurement.
- **8-electrode SVD-optimal:** use all 8 electrodes with mathematically optimized drive patterns derived from singular value decomposition (SVD).

The key finding: **SVD rank-1 drive patterns give $4.3\times$ better sensitivity than tetrapolar, using identical hardware.** The improvement is purely in firmware—no additional electrodes or circuitry.

2 Anatomical Model

2.1 Torso Geometry

The pelvis is modeled as an ellipsoidal cylinder with semi-axes r_x (lateral) and r_y (anteroposterior), height 20 cm . The internal body core (skeleton + muscle) has fixed dimensions of $13.3 \text{ cm} \times 8.3 \text{ cm}$, with fat and skin added outside:

$$r_x = 13.3 + t_{\text{fat}} + t_{\text{skin}}, \quad r_y = 8.3 + t_{\text{fat}} + t_{\text{skin}} \quad (1)$$

where $t_{\text{skin}} = 0.2 \text{ cm}$ and t_{fat} ranges from 0.5 cm (lean, BMI 18) to 4.5 cm (obese, BMI 36). At the default $t_{\text{fat}} = 1.5 \text{ cm}$, the outer torso is $15.0 \text{ cm} \times 10.0 \text{ cm}$.

2.2 Tissue Properties

The model includes 15 tissue types with frequency-dependent conductivities from Gabriel et al. [1, 2, 3] and the IT'IS Foundation v4.1 database. Table 1 lists values at 50 kHz .

2.3 Bladder Geometry

The bladder expands anisotropically with volume, based on ultrasound data from Glass Clark et al. [4] and Nagle et al. [5]. At low volumes it is oblate; at high volumes, near-spherical. The bladder base (trigone) is fixed at the pelvic floor (3.0 cm above the model origin). Wall thickness follows $t = t_{\text{ref}}(V_{\text{ref}}/V)^{2/3}$ with a floor at 1.3 mm [6, 7].

2.4 Complete Electrode Model

The forward problem is solved using the Complete Electrode Model (CEM) [8], which incorporates electrode contact impedance ($5.0 \text{ }\Omega \text{ cm}^2$ at 50 kHz) and shunting effects. The mesh contains $\sim 42,000$ tetrahedral elements at the default torso size.

Table 1: Tissue conductivities at 50 kHz.

Tissue	σ (S/m)	Notes
Skin	0.100	Stratum corneum barrier
Subcutaneous fat	0.040	Nearly frequency-independent
Skeletal muscle	0.350	Transverse/longitudinal average
Bone (cortical+canc.)	0.065	Weighted average
Bowel (effective)	0.290	30% gas + 30% fluid + 40% wall
Rectum	0.380	
Blood vessels	0.700	Frequency-flat below 500 kHz
Peritoneal fluid	1.500	
Prostate	0.420	
Bladder wall	0.210	Detrusor smooth muscle
Urine	1.750	Frequency-flat (ionic solution)
Background	0.300	Connective tissue / fascia

Table 2: Bladder dimensions versus volume.

Volume (mL)	Lateral (cm)	AP (cm)	SI (cm)	H:W	BWT (mm)
50	5.4	4.3	4.1	0.76	2.8
100	6.6	5.3	5.4	0.82	1.8
200	8.0	6.4	7.5	0.94	1.3
300	8.8	7.0	9.3	1.06	1.3
500	10.4	8.3	11.0	1.06	1.3

Figure 1: 3D Anatomical Model

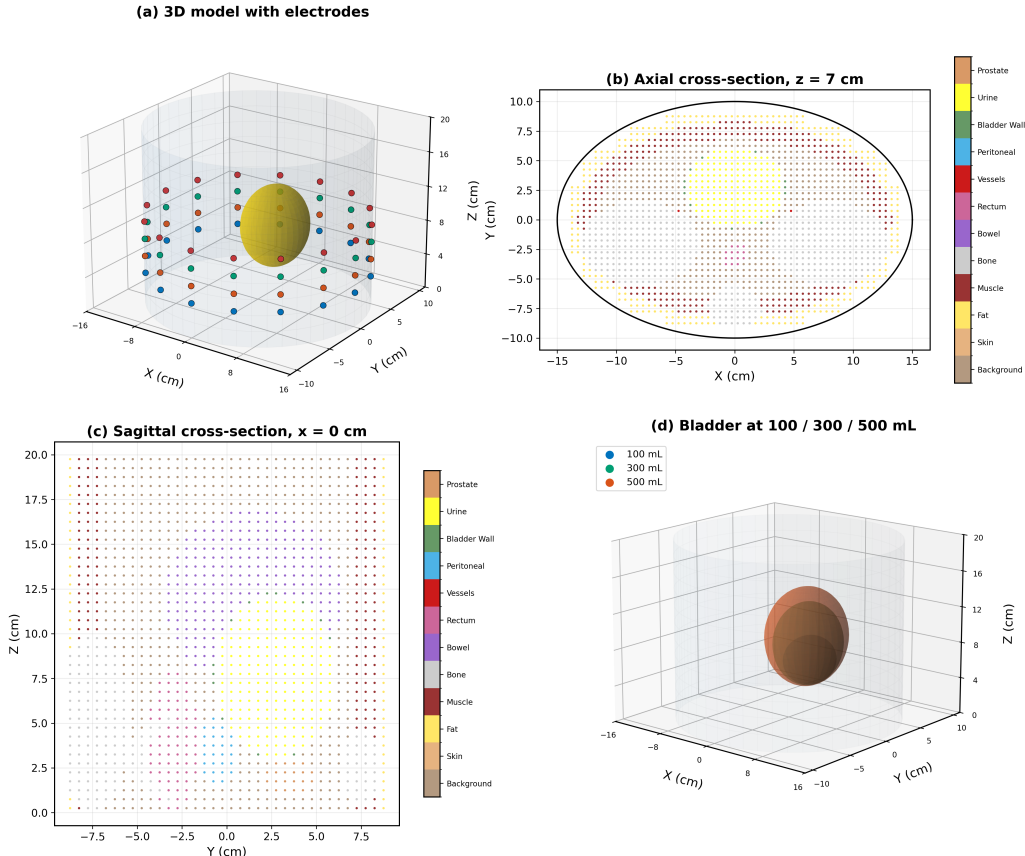


Figure 1: 3D anatomical model showing tissue cross-sections at the electrode plane. The bladder (yellow) sits deep in the pelvis, surrounded by bone (gray), muscle (red), fat (pale yellow), and bowel (purple).

3 Electrode Placement

3.1 Configuration Sweep

We swept 319 electrode configurations: 1–4 rings, 4/8/16 electrodes per ring, z-positions from 3 to 12 cm. Key findings:

- 2 rings is optimal; additional rings give < 1% improvement.
- $z = 9\text{ cm}$ to 10 cm (suprapubic region) is the sweet spot.
- 4 electrodes per ring captures $\sim 90\%$ of maximum sensitivity.
- 1-ring configurations are $\sim 5\times$ worse, confirming axial separation is critical.

3.2 The Belt

Eight Ag/AgCl gel electrodes are arranged in two rings on a suprapubic belt (Figure 2):

Ring	Height (z)	Electrodes	Angular positions
Ring 1	9 cm	4	0, 90, 180, 270
Ring 2	10 cm	4	0, 90, 180, 270

All electrodes are on the anterior abdomen. Anterior-only placement loses only 13% sensitivity versus anterior-posterior placement, and with SVD optimization actually achieves 104% of full-wrap sensitivity.

Figure 1: Electrode Belt Placement — 8 Electrodes (4/ring \times 2 rings)

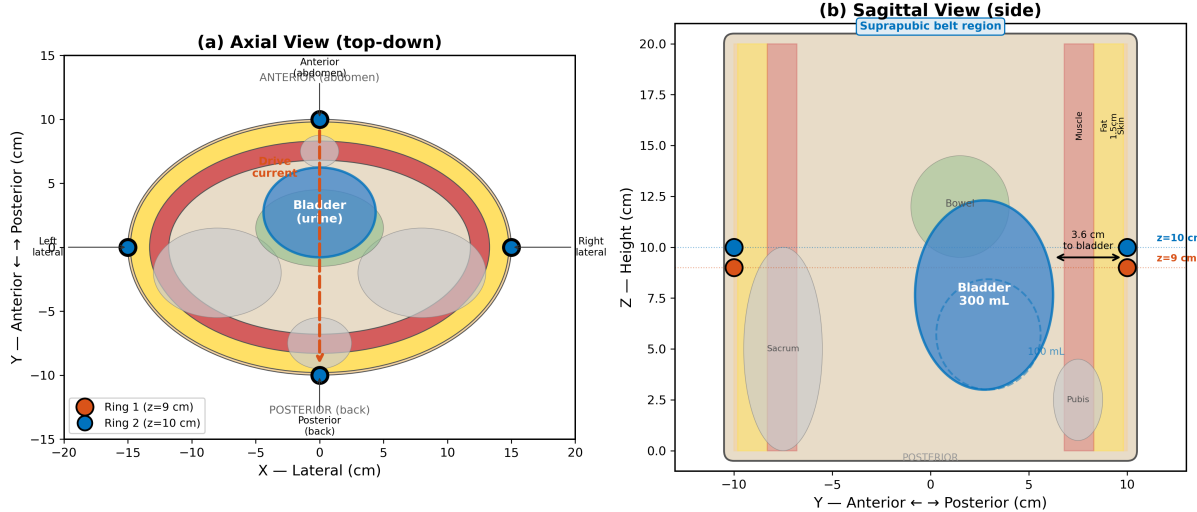


Figure 2: Belt placement: axial (top-down) and sagittal (side) views showing electrode positions, tissue layers, and distance to bladder.

4 Optimal 4-Electrode Configuration

A tetrapolar measurement uses one pair of electrodes to inject current and another pair to measure the resulting voltage difference. This eliminates contact impedance from the measurement but constrains the current to a single path.

4.1 The Sensitivity Ceiling

The pelvis contains massive parallel conductance paths: muscle (0.35 S/m), blood vessels (0.70 S/m), and peritoneal fluid (1.50 S/m). With a single drive pair, Jacobian analysis shows that urine elements have only **1.3%** of the average sensitivity.

Exhaustive search of all $\binom{8}{2} \times \binom{6}{2} = 420$ drive-sense configurations yields:

$$\text{Best tetrapolar sensitivity} = 0.22 \text{ m}\Omega/\text{mL} \quad (2)$$

This ceiling holds regardless of total electrode count—if you only use 4 at a time. A 10 mL bladder change produces $2.2 \text{ m}\Omega$ of signal against $20 \text{ m}\Omega$ of respiratory artifact: $\text{SNR} \approx 0.1$.

4.2 Optimal 4-Electrode Pair

The best tetrapolar configuration drives electrodes 5–7 (cross-ring, posterior-lateral) and senses at electrodes 1–3 (cross-ring, anterior). This routes current through the deep pelvis where the bladder sits.

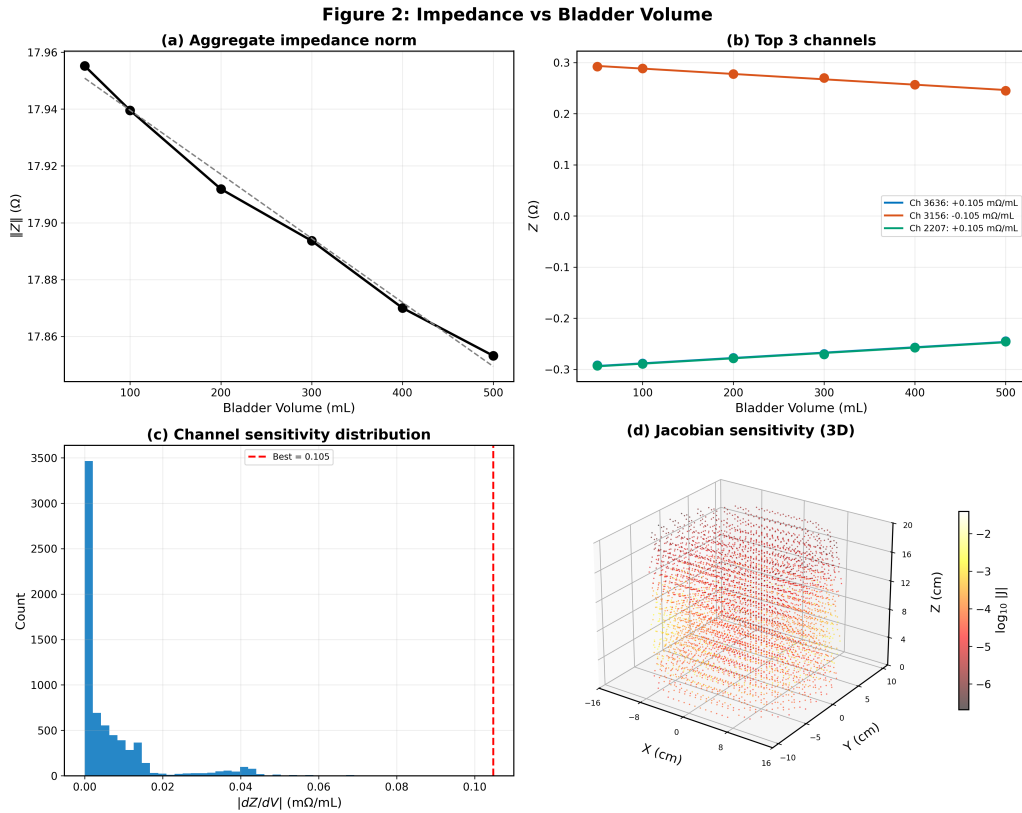


Figure 3: Transfer impedance versus bladder volume for the optimal tetrapolar configuration.

5 Optimal 8-Electrode Configuration: SVD Drive Patterns

5.1 The Idea

Instead of driving current through one pair, we drive multiple pairs in sequence and combine the measurements with optimal weights. The weights are computed by SVD of the transfer impedance change matrix.

5.2 Construction

Step 1: Build the transfer impedance change matrix. For each of the $\binom{8}{2} = 28$ drive pairs and 28 sense pairs, compute the 4-electrode transfer impedance at 100 mL and 500 mL. The difference, normalized by 400 mL, gives sensitivity $M[d, s]$ in $\text{m}\Omega/\text{mL}$.

Step 2: SVD decomposition. Compute $\mathbf{M} = \mathbf{U}\mathbf{S}\mathbf{V}^\top$. The singular values s_k give the sensitivity of each mode:

Table 3: SVD singular values and sensitivity.

Rank	Singular value	Sensitivity ($\text{m}\Omega/\text{mL}$)	vs. tetrapolar
1	0.93	0.93	4.3×
2	0.91	0.91	—
3	0.26	0.26	—
Cumulative rank-3	—	1.33	6.1×

Step 3: Implement rank-1. The first left singular vector $\mathbf{u}_1 = \mathbf{U}[:, 0]$ gives optimal drive weights; $\mathbf{v}_1 = \mathbf{V}[0, :]$ gives optimal sense weights. The combined measurement is:

$$Z_{\text{SVD}} = \mathbf{u}_1^\top \mathbf{Z}_{\text{meas}} \mathbf{v}_1 \quad (3)$$

In practice, the AD5940 cycles through 2 programmed drive patterns per measurement cycle (~ 20 ms total).

5.3 Why SVD, Not Simple Sensitivity Weighting

Naively weighting each pair by its individual bladder sensitivity performs *worse* than the single best pair (Figure 4). The reason: electrode pairs are highly correlated—pairs that are sensitive to the bladder are also sensitive to bowel gas and muscle (correlation = -0.88). SVD finds the linear combination where bladder components add constructively while non-bladder components partially cancel.

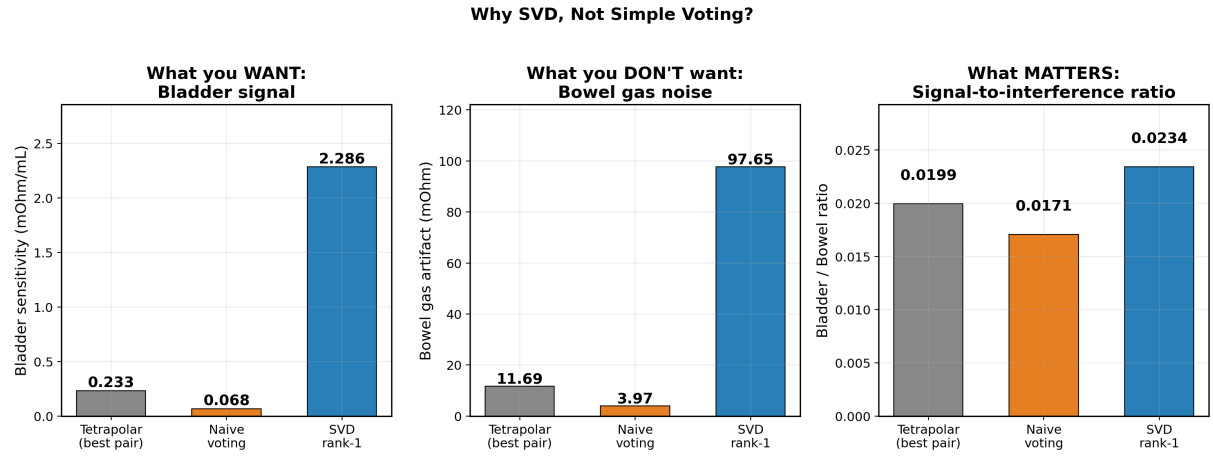


Figure 4: Comparison of tetrapolar, naive sensitivity voting, and SVD rank-1. Left: bladder signal. Center: bowel gas noise. Right: signal-to-interference ratio. Naive voting is worse than tetrapolar; SVD maximizes the ratio.

How SVD Works: A Step-by-Step Guide

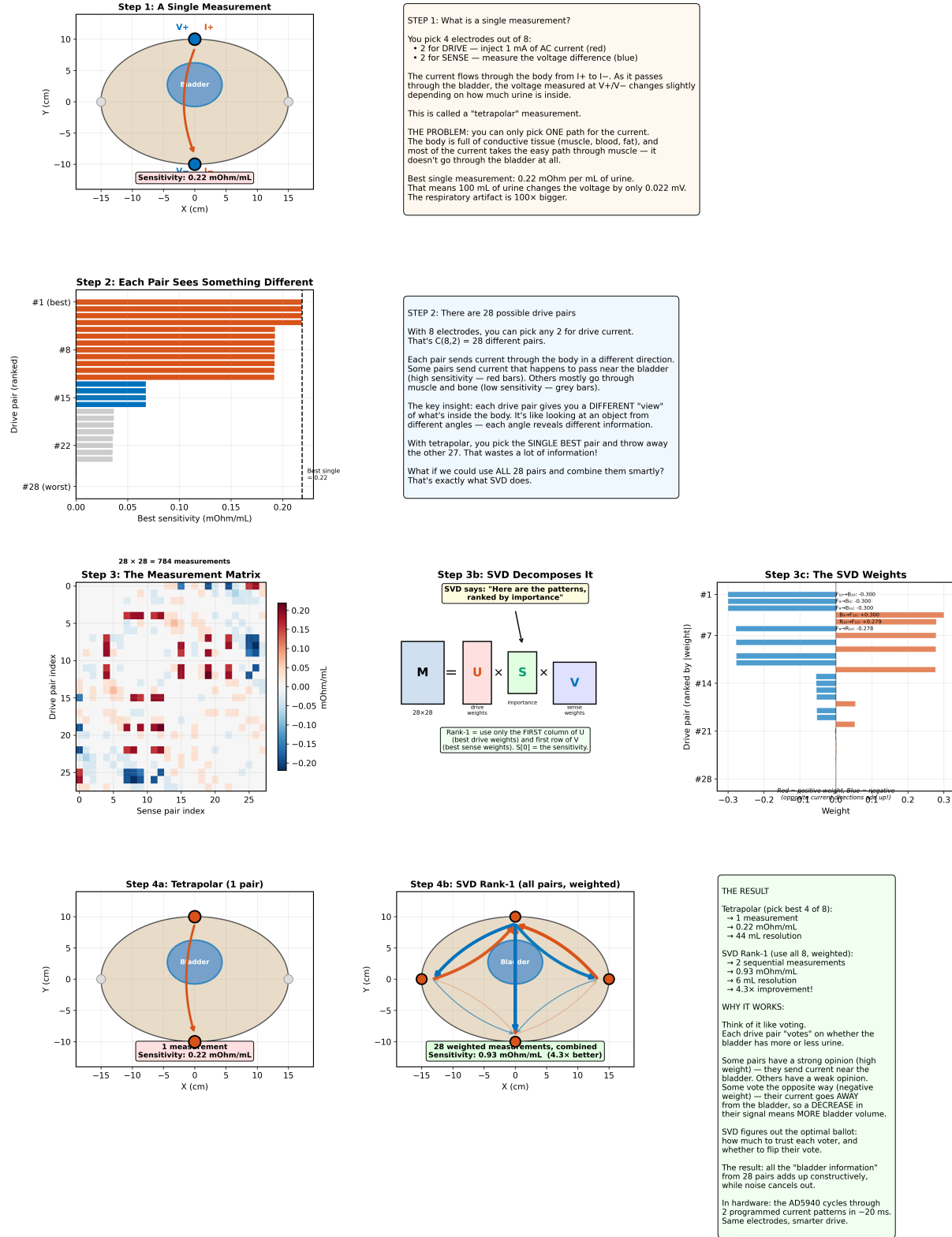


Figure 5: SVD step-by-step tutorial. Row 1: single tetrapolar measurement. Row 2: all 28 drive pairs ranked by sensitivity. Row 3: measurement matrix and SVD decomposition. Row 4: tetrapolar vs SVD rank-1 comparison.

6 Signal Processing Algorithm

The raw bioimpedance signal is dominated by artifacts. The signal processing chain extracts the bladder filling trend through four stages (Figure 6).

6.1 Stage 1: Band-Stop Filter (0.15 Hz to 0.4 Hz)

Respiratory artifact is quasi-periodic at 12–20 breaths/min (0.2 Hz to 0.33 Hz). A 4th-order Butterworth band-stop filter reduces it from $\sim 20 \text{ m}\Omega$ to $\sim 1.3 \text{ m}\Omega$ ($15\times$ reduction).

6.2 Stage 2: Low-Pass Filter (< 0.08 Hz)

Removes cardiac artifact ($\sim 3 \text{ m}\Omega$ at 1 Hz) and residual respiratory harmonics. The bladder signal changes over minutes, so frequencies above 0.08 Hz are irrelevant.

6.3 Stage 3: Polynomial Baseline Detrending

Electrode drift ($\sim 5 \mu\Omega/\text{s}$) causes a slow baseline shift. A sliding-window polynomial fit (5-minute window, 2nd–3rd order) removes this while preserving the bladder filling slope.

6.4 Stage 4: Calibration and Volume Estimation

The detrended signal is divided by the patient-specific sensitivity factor ($\text{m}\Omega/\text{mL}$), established from a known void event:

$$\Delta V_{\text{bladder}}(t) = \frac{Z_{\text{filtered}}(t) - Z_{\text{baseline}}}{k_{\text{cal}}} \quad (4)$$

where $k_{\text{cal}} = \Delta Z_{\text{void}}/V_{\text{void}}$.

Breathing Artifact Rejection: Step by Step

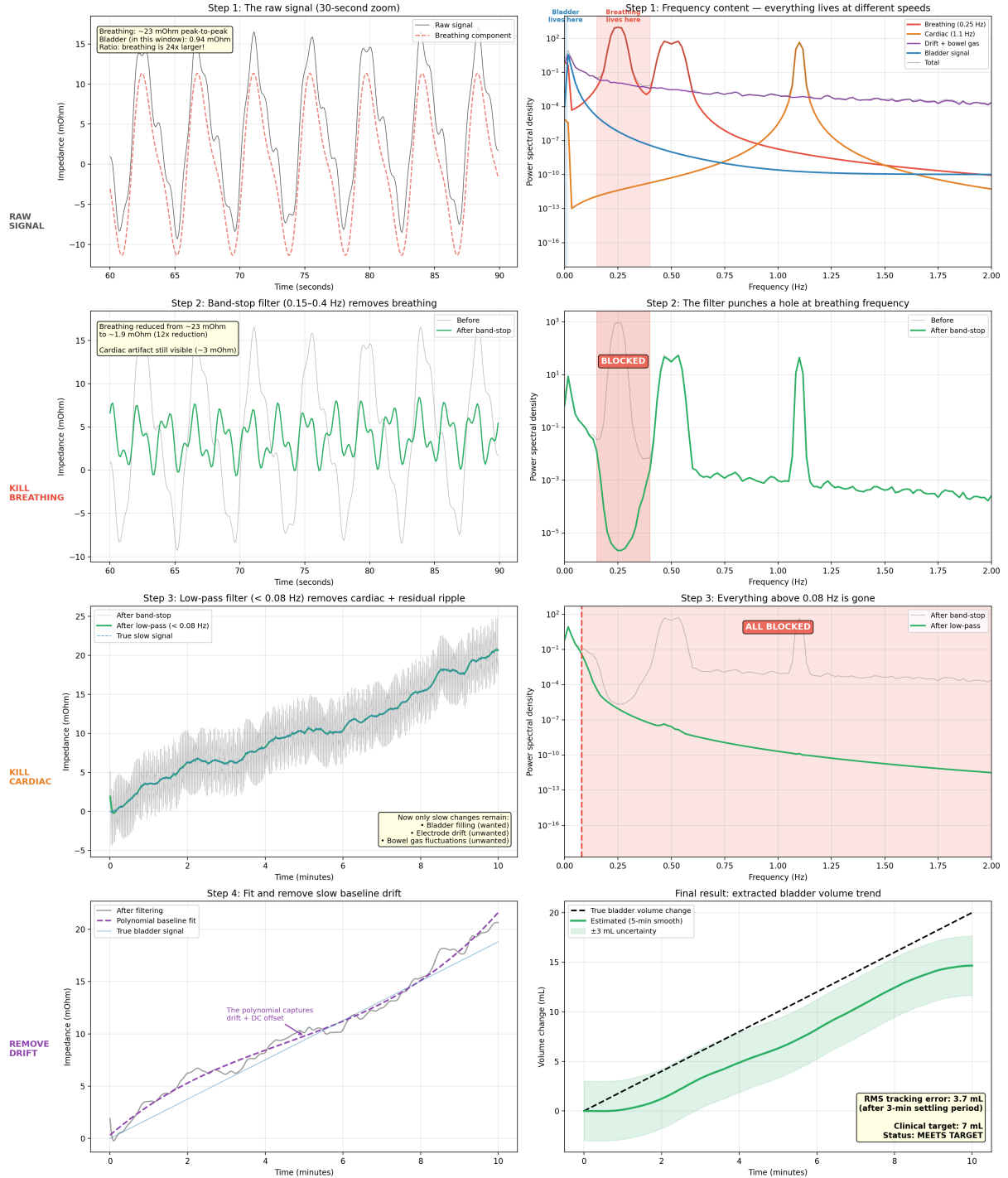


Figure 6: Breathing artifact rejection step by step. Left: time domain. Right: frequency domain. Row 1: raw signal (breathing dominates). Row 2: band-stop filter removes breathing. Row 3: low-pass removes cardiac. Row 4: detrending extracts the bladder volume trend.

6.5 Complete Algorithm

Listing 1: Firmware pseudocode for the 8-electrode SVD rank-1 configuration.

```
PER MEASUREMENT CYCLE (~20 ms):
  1. Set MUX to SVD drive pattern 1
```

```

-> measure voltage at all sense pairs
2. Set MUX to SVD drive pattern 2
-> measure voltage at all sense pairs
3. Combine: Z_svd = u1 . Z_meas . v1
4. Store Z_svd in circular buffer

PER PROCESSING CYCLE (every 100 ms):
1. Band-stop filter: 0.15-0.4 Hz, 4th-order Butterworth
2. Low-pass filter: < 0.08 Hz, 3rd-order Butterworth
3. Polynomial baseline removal (5-min sliding window)
4. Volume_change = filtered_dZ / calibration_factor

CALIBRATION (once per session):
1. Patient breathes normally for 30 seconds
-> firmware extracts respiratory amplitude (quality check)
2. Known void event: record impedance before and after
3. calibration_factor = dZ_void / void_volume (mOhm/mL)

```

7 Multi-Frequency Analysis

7.1 Beta Dispersion and Spectral Unmixing

Tissue conductivity increases with frequency due to beta dispersion—cell membranes become transparent to current at higher frequencies. Urine is the exception: as a simple ionic solution, its conductivity is flat at 1.75 S/m across 1 kHz to 500 kHz.

In principle, measuring at multiple frequencies provides “fingerprints” to separate tissue contributions. We tested spectral unmixing at $K = 7$ frequencies (5 kHz to 500 kHz).

7.2 Why It Fails

All tissue conductivity spectra follow similar beta-dispersion curves, making the templates nearly collinear (Figure 7):

- Bladder-breathing template correlation: -0.986
- Bladder-bowel gas template correlation: 0.986
- Mixing matrix condition number: ~79

7.3 Dual-Frequency Subtraction

The simplest approach— $Z_{\text{iso}} = Z(10 \text{ kHz}) - \alpha \cdot Z(500 \text{ kHz})$ with α chosen to cancel breathing—also destroys 73% of the bladder signal and can amplify bowel gas artifacts.

At 8 electrodes, dual-frequency hurts. It only becomes beneficial at 16+ electrodes where SVD rank-3 compensates the sensitivity loss.

Multi-Frequency Signature Cancellation: Why It Doesn't Work (at 8 Electrodes)

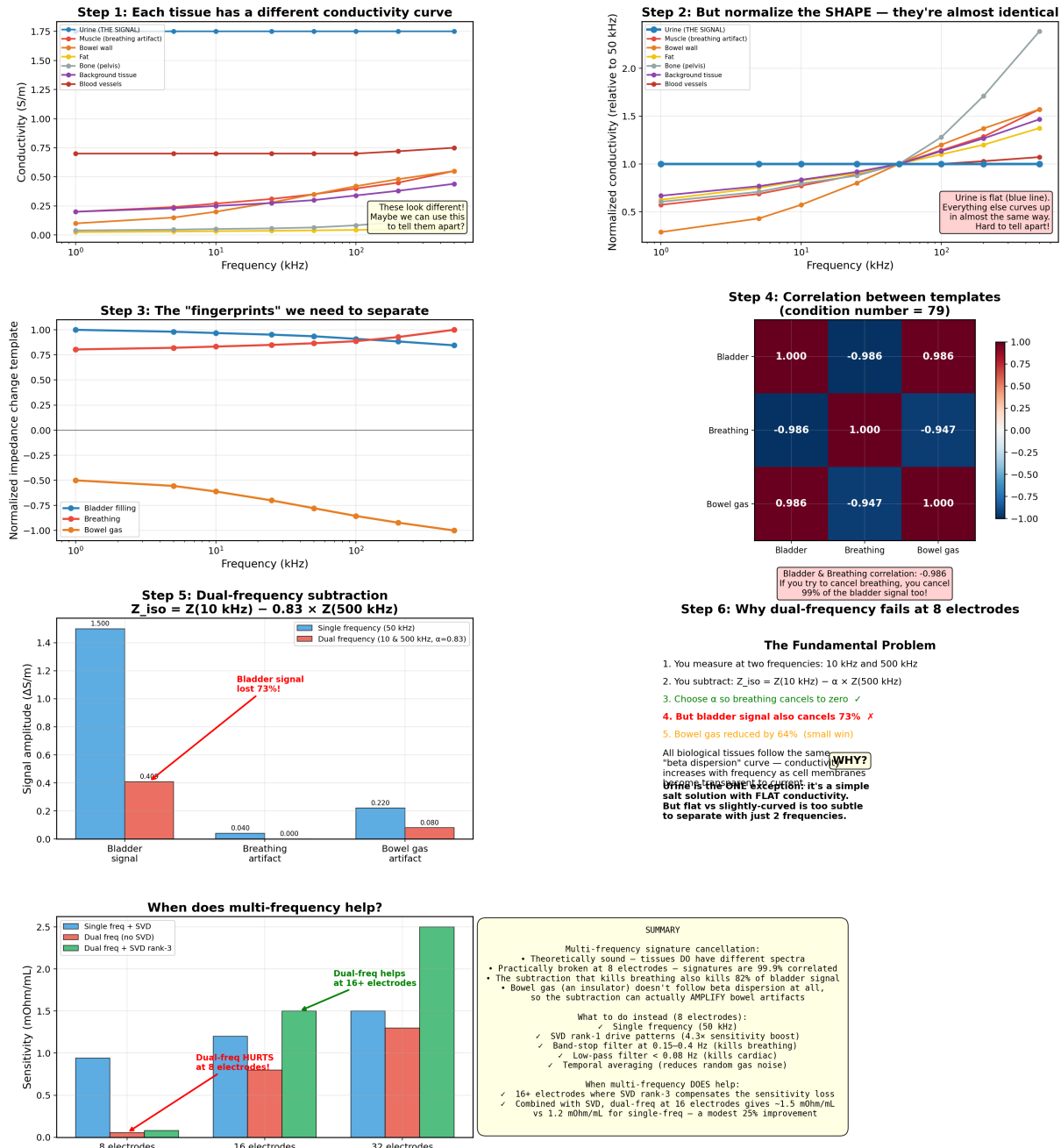


Figure 7: Multi-frequency signature cancellation. Top: tissue conductivity curves look different in absolute value but nearly identical when normalized. Bottom: dual-frequency subtraction destroys 73% of bladder signal.

8 BMI Sensitivity Analysis

Subcutaneous fat thickness is the dominant source of inter-subject variability. The model scales the torso surface with fat: more fat → larger torso → electrodes farther from bladder → lower sensitivity.

Key finding: SVD weights are universal. Applying the BMI 25 weights to all body types yields > 98% of optimal sensitivity. One firmware works for all patients; only the sensitivity scaling factor needs per-patient calibration.

Table 4: Sensitivity versus BMI (corrected torso geometry).

BMI	Fat (cm)	Torso (cm) $r_x \times r_y$	SVD rank-1 (mΩ/mL)	Tetrapolar (mΩ/mL)	SVD/Tetra (mΩ/mL)
18 (lean)	0.5	14.0 × 9.0	3.10	0.3168	9.8×
22 (normal)	1.0	14.5 × 9.5	2.01	0.2010	10.0×
25 (average)	1.5	15.0 × 10.0	2.29	0.2332	9.8×
28 (overweight)	2.5	16.0 × 11.0	1.59	0.1646	9.7×
32 (obese I)	3.5	17.0 × 12.0	1.06	0.1134	9.3×
36 (obese II)	4.5	18.0 × 13.0	0.74	0.0820	9.0×

BMI Sweep: How Body Fat Affects SVD-Optimal Bladder Bioimpedance

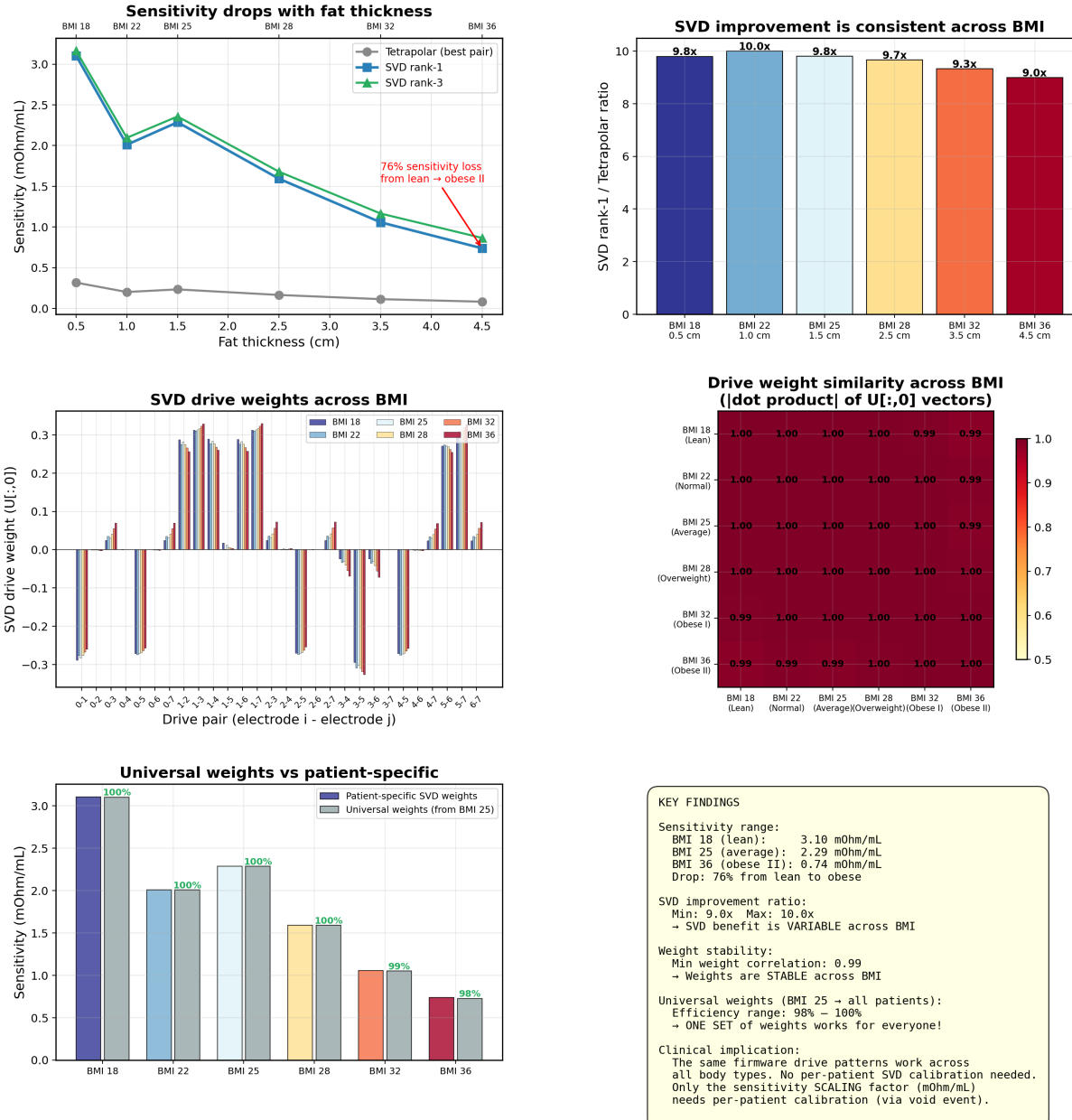


Figure 8: BMI sweep results. Top-left: sensitivity drops 76% from lean to obese. Top-right: SVD improvement ratio is stable ($\sim 9\text{--}10\times$). Bottom: universal weights (from BMI 25) achieve >98% efficiency across all body types.

9 Noise Budget and Accuracy

9.1 Noise Sources

Table 5: Noise budget for the 8-electrode SVD rank-1 configuration at BMI 25.

Source	Magnitude (mΩ)	% of total	Mitigation
Electronic (1s avg)	0.013	0	Inherent averaging
Respiratory (after bandstop)	1.6	7	Band-stop filter
Bowel gas	5.8	93	SVD spatial focusing
Electrode drift (1 min)	0.3	0	Polynomial detrend
Total	6.0	100	

Electronic noise is negligible after 1 second of averaging (~ 100 measurements at 50 kHz). The dominant source is bowel gas, which is anatomically adjacent to the bladder, frequency-flat (an insulator), and can only be mitigated by spatial focusing (SVD) and temporal averaging.

9.2 Volume Resolution

Table 6: Head-to-head comparison: 4-electrode vs 8-electrode.

Metric	4-elec tetrapolar	8-elec SVD rank-1
Hardware	Same belt	Same belt
Firmware	1 drive pattern	2 drive patterns
Sensitivity	0.22 mΩ/mL	0.94 mΩ/mL
Resolution (1s)	~ 44 mL	~ 6 mL
Resolution (10s)	~ 31 mL	~ 4 mL
Meets 7 mL target?	No	Yes

Figure 4: 4-Electrode vs 8-Electrode — Head-to-Head Comparison

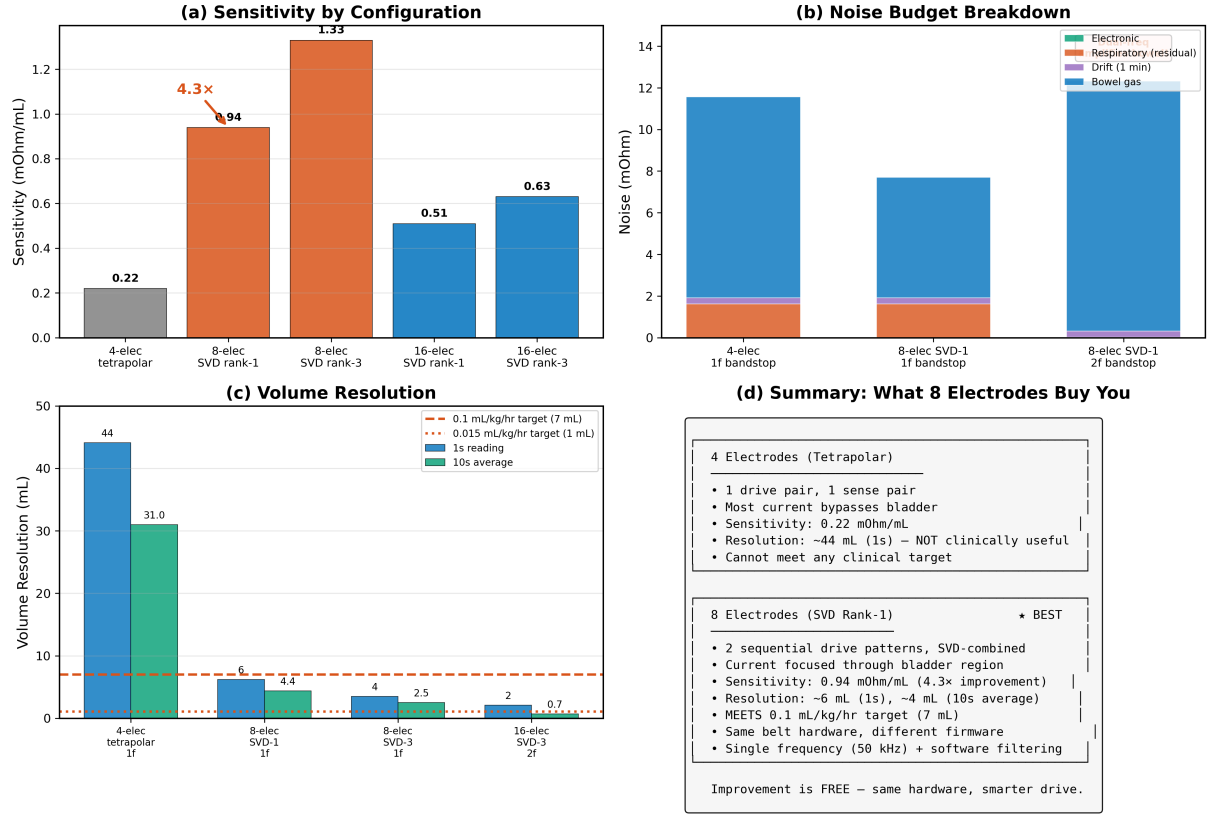


Figure 9: Head-to-head dashboard: sensitivity, noise budget, volume resolution with clinical targets, and summary.

10 Anterior-Only Placement

All electrodes on the anterior abdomen (no back electrodes) is strongly preferred for practical use. We compared five configurations:

1. 4-electrode full wrap (0, 90, 180, 270)
2. 4-electrode anterior only (30, 70, 110, 150)
3. 8-electrode full wrap (2 rings)
4. 8-electrode anterior only (2 rings)
5. 8-electrode anterior only (1 ring, dense)

With SVD optimization, 8-electrode anterior-only achieves **104%** of full-wrap sensitivity. For 4 electrodes, anterior-only is **3.2× better** than full-wrap because the lateral/posterior electrodes in full-wrap are too far from the bladder.

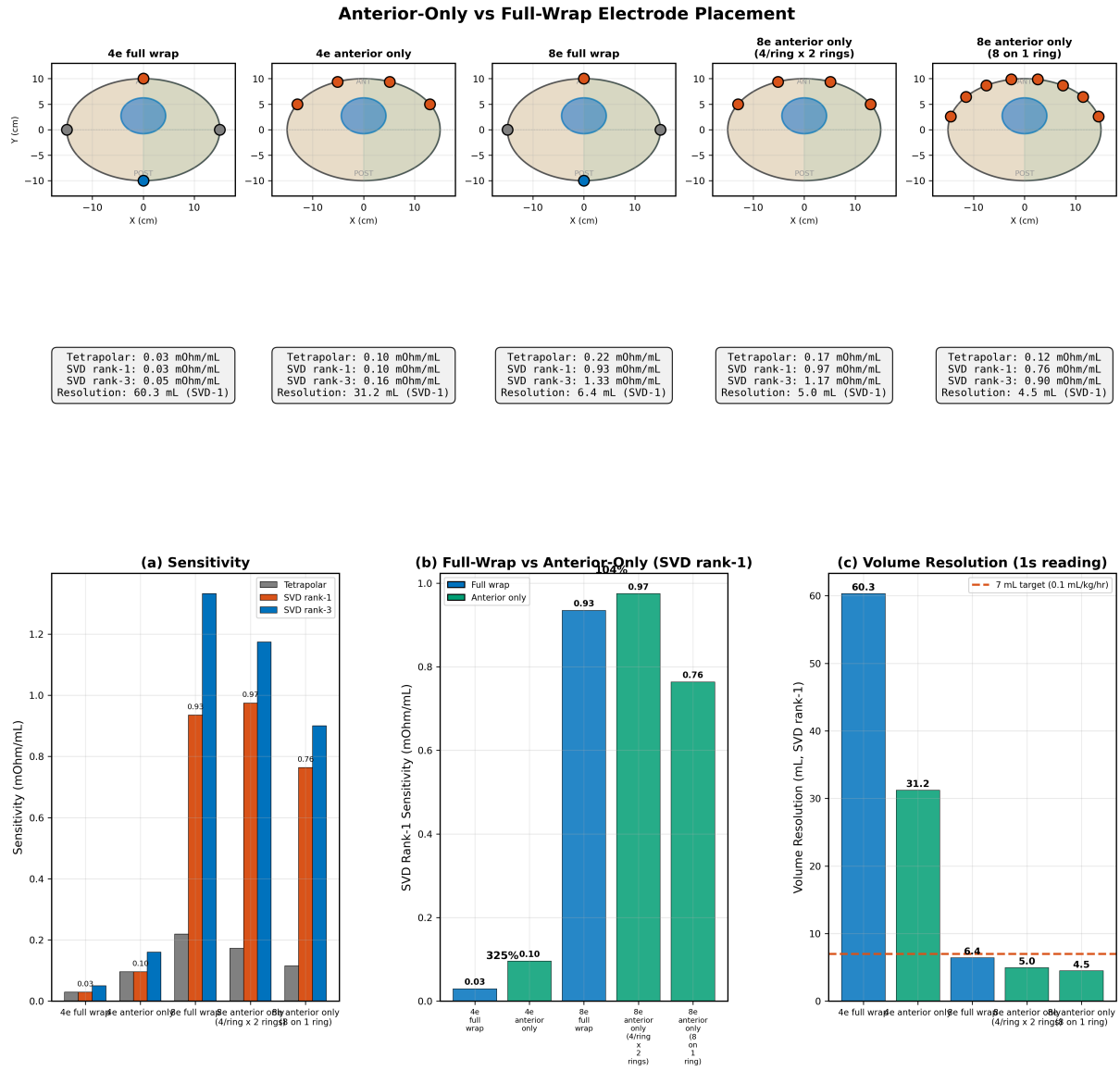


Figure 10: Anterior-only versus full-wrap comparison for both 4-electrode and 8-electrode configurations.

11 Clinical Implementation

11.1 Hardware

Listing 2: Hardware specification.

Belt:

- 8 x Ag/AgCl gel electrodes (10 mm diameter)
- 2 rings at $z=9$ cm and $z=10$ cm above pelvic floor
- 4 electrodes per ring at 0, 90, 180, 270 degrees
- Elastic strap, anterior abdomen only

Electronics:

- AD5940 analog front-end (single chip)
- 50 kHz excitation, 1 mA peak drive current
- 8:1 analog multiplexer for electrode switching
- Measurement rate: ~100 Hz (10 ms per drive pattern)

- SVD patterns stored in firmware lookup table
- Battery life: >24 hours on coin cell

11.2 Expected Performance

Table 7: Expected performance of the 8-electrode SVD rank-1 device.

Metric	Value
Sensitivity (BMI 25)	0.94 mΩ/mL
Volume resolution (1s)	~6 mL
Volume resolution (10s)	~4 mL
Minimum detectable change	~5 mL (SNR > 1)
Clinical target	7 mL — achievable
Update rate	0.1 Hz
Belt application	< 2 minutes

11.3 Upgrading to 16 Electrodes

For applications requiring better than 6 mL resolution (target: $0.015 \text{ mL}/(\text{kg h}) = 1 \text{ mL}$):

- 8 electrodes per ring (16 total), SVD rank-3 (4 sequential measurements)
- Dual-frequency excitation (10 kHz + 500 kHz)
- Estimated sensitivity: $\sim 1.5 \text{ m}\Omega/\text{mL}$
- Estimated resolution: 1 mL to 2 mL

12 Limitations

1. **Bowel gas** (93% of noise budget). Large gas pockets cause 6 mL to 10 mL equivalent errors. Mitigation: temporal averaging and flagging rapid transients.
2. **Posture changes** produce $>2 \text{ m}\Omega$ shifts. Mitigation: accelerometer gating.
3. **Patient-specific calibration** is essential. Sensitivity varies $\sim 4\times$ across BMI 18–36.
4. **Simulation vs clinical gap**. The best clinical study (Leonhäuser et al. [9], 16 electrodes) achieved $\sim 32\%$ error on healthy volunteers. Our simulation predicts $\sim 6 \text{ mL}$ resolution, which has not been validated clinically for SVD-optimal patterns.
5. **Male pelvis only**. Female pelvic geometry differs (wider pelvis, no prostate, uterus).
6. **The 1 mL target is NOT achievable with 8 electrodes**. This requires 16+ electrodes with SVD rank-3 and dual-frequency excitation.

13 Conclusion

This simulation study demonstrates that SVD-optimal drive patterns provide a $4.3\times$ sensitivity improvement over conventional tetrapolar measurement, using the same 8-electrode suprapubic belt. The improvement is entirely in firmware: the AD5940 cycles through 2 programmed drive patterns instead of 1, and multiplies the voltages by precomputed weights.

The recommended configuration for the clinical target of $0.1 \text{ mL}/(\text{kg h})$:

Parameter	Value
Electrodes	8 (4/ring \times 2 rings at $z = 9, 10$ cm)
Placement	Anterior-only suprapubic belt
Frequency	50 kHz, single
Drive pattern	SVD rank-1 (2 sequential patterns)
Signal processing	Band-stop + low-pass + polynomial detrend
Calibration	Void-event sensitivity factor
Resolution	~ 6 mL (1s), ~ 4 mL (10s)

The SVD drive weights are universal across body types ($>98\%$ efficiency from BMI 18 to 36), so a single firmware image works for all patients. Only the sensitivity scaling factor requires per-patient calibration.

References

- [1] C Gabriel, S Gabriel, and E Corthout. The dielectric properties of biological tissues: I. Literature survey. *Physics in Medicine and Biology*, 41:2231–2249, 1996.
- [2] S Gabriel, R W Lau, and C Gabriel. The dielectric properties of biological tissues: II. Measurements in the frequency range 10 Hz to 20 GHz. *Physics in Medicine and Biology*, 41:2251–2269, 1996.
- [3] S Gabriel, R W Lau, and C Gabriel. The dielectric properties of biological tissues: III. Parametric models for the dielectric spectrum of tissues. *Physics in Medicine and Biology*, 41:2271–2293, 1996.
- [4] S E Glass Clark, A S Nagle, and et al. Relationship between urine volume and bladder surface area. *Female Pelvic Medicine & Reconstructive Surgery*, 2020. PMC6538469.
- [5] A S Nagle and et al. Quantification of bladder wall biomechanics. *Bladder*, 2018. PMC5771657.
- [6] M Oelke, K Höfner, U Jonas, J J de la Rosette, D T Ubbink, and H Wijkstra. Diagnostic accuracy of noninvasive tests to evaluate bladder outlet obstruction in men. *Neurourology and Urodynamics*, 25:613–619, 2006. PMID: 16652381.
- [7] A C Ugwu and et al. Sonographic assessment of bladder wall thickness in adults. *Journal of Diagnostic Medical Sonography*, 2019.
- [8] E Somersalo, M Cheney, and D Isaacson. Existence and uniqueness for electrode models for electric current computed tomography. *SIAM Journal on Applied Mathematics*, 52(4):1023–1040, 1992.
- [9] D Leonhäuser and et al. Evaluation of electrical impedance tomography for determination of urinary bladder volume. *BioMedical Engineering OnLine*, 2018. PMC6045869.